Simple Turbulence Models for Supersonic Flows: Bodies at Incidence and Compression Corners

Siamack A. Shirazi* and C. Randall Truman†
University of New Mexico, Albuquerque, New Mexico 87131

Parabolized Navier-Stokes (PNS) predictions of turbulent flows at supersonic and hypersonic speeds past two sphere-cones and a cone-cylinder-flare are used to evaluate simple turbulence models. Modifications to an algebraic turbulence model are proposed to improve predictions for flow on bodies at incidence. Predictions using a simple modification for the length scale and a model based upon Bradshaw's extra-strain-rate hypothesis are compared with measurements of supersonic and hypersonic flows. The modifications lead to significant improvements in predicted wall shear stress for a Mach 3 flow over a sphere-cone at moderate angle of attack. In addition, predictions of hypersonic flow past a cone-cylinder-flare are used to compare the algebraic Cebeci-Smith turbulence model with the nonequilibrium Johnson-King half-equation model. Predictions are compared with measurements of surface pressure and heat transfer for isothermal-wall flow at Mach 9.22 for a cone-cylinder-flare. The algebraic model predictions are quite satisfactory and no significant improvement is achieved with the nonequilibrium model for this flow with no streamwise separation.

Nomenclature

$\tilde{a}_\infty$ = freestream speed of sound
$A^+, \mathbf{A}^+$ = empirical constants in the van Driest damping, Eqs. (4) and (17)
D = van Driest damping, Eqs. (4) and (17)
K_e = dimensionless effective conductivity, $\tilde{K}_e/\tilde{K}_\infty$, Eq. (2)
$\tilde{L}$ = characteristic or reference length
M = freestream Mach number, $\tilde{V}_\infty/\tilde{a}_\infty$
N = dimensionless normal distance from wall, $\tilde{N}/\tilde{L}$
N^+ = dimensionless wall coordinate, Eq. (5)
p = dimensionless pressure, $\tilde{p}/\tilde{\rho}_\infty\tilde{V}_\infty^2$
Pr = Prandtl number
r = radial distance from body axis, Eq. (8)
Re_∞ = freestream Reynolds number, $\tilde{\rho}_\infty\tilde{V}_\infty\tilde{L}/\tilde{\mu}_\infty$
St_∞ = Stanton number based on freestream conditions, Eq. (25)
$\tilde{T}$ = temperature
u,v,w = dimensionless velocity components in the Cartesian coordinates (x,y,z), $\tilde{u}/\tilde{V}_\infty$, $\tilde{v}/\tilde{V}_\infty$, $\tilde{w}/\tilde{V}_\infty$
U = dimensionless velocity tangent to the surface (excluding crossflow), $\tilde{U}/\tilde{V}_\infty$
V = dimensionless total velocity, $(u^2+v^2+w^2)^{1/2}$
V_T = dimensionless velocity tangent to the surface (including crossflow), $\tilde{V}_T/\tilde{V}_\infty$
$\tilde{V}_\infty$ = freestream total velocity
W = dimensionless crossflow velocity, $\tilde{W}/\tilde{V}_\infty$
x,y,z = dimensionless physical Cartesian coordinates, $\tilde{x}/\tilde{L}, \tilde{y}/\tilde{L}, \tilde{z}/\tilde{L}$
α = angle of attack
γ = Klebanoff intermittency factor, Eq. (9)
δ^* = dimensionless kinematic, or "incompressible," displacement thickness, Eq. (7)
θ_c = cone half-angle
κ = von Kármán constant
μ = dimensionless coefficient of viscosity, $\tilde{\mu}/\tilde{\mu}_\infty$
μ_t = dimensionless eddy viscosity, $\tilde{\mu}_t/\tilde{\mu}_\infty$
μ_e = dimensionless effective viscosity, $\tilde{\mu}_e/\tilde{\mu}_\infty$, Eq. (1)
ξ,η,ζ = dimensionless computational coordinates in the streamwise (axial), radial (normal), and circumferential directions
ρ = dimensionless density, $\tilde{\rho}/\tilde{\rho}_\infty$
τ = dimensionless total Reynolds shear stress (divided by density), Eq. (16)
τ_w = dimensionless wall shear stress, $\tilde{\tau}_w/(\tilde{\mu}_\infty\tilde{V}_\infty/\tilde{L})$
ϕ = meridian angle, $\phi=0$ deg windward, $\phi=180$ deg leeward

Subscripts and Superscripts

∞ = freestream
e = edge of boundary layer
eq = equilibrium value
m = location of maximum in τ
ti = inner region of turbulent boundary layer
to = outer region of turbulent boundary layer
w = wall or surface value
$(\tilde{\ })$ = dimensional quantity

Introduction

In recent years, there has been growing interest in the prediction of supersonic and hypersonic turbulent flows past bodies at incidence and flows that exhibit shock/boundary-layer interactions. Algebraic (or zero-equation) turbulence models are attractive for Navier-Stokes (NS) or parabolized Navier-Stokes (PNS) methods since the required storage and computational time are significantly less than those using more sophisticated turbulence models for supersonic and hypersonic flows.[1-4] Two different types of flows were examined in the present work. In the first part, flows past slender bodies at incidence are considered. A study of flows past compression corners then follows.

Flows past Slender Bodies at Incidence

Many predictions of supersonic and hypersonic flows past bodies at incidence have reported problems in determining the outer length scale in algebraic turbulence models in the leeward

Presented as Paper 89-0669 at the AIAA 27th Aerospace Sciences Meeting, Reno, NV, Jan. 1989; received Aug. 14, 1989; revision received Aug. 15, 1990; accepted for publication Aug. 31, 1990.

*Research Associate, Department of Mechanical Engineering; currently Assistant Professor, Department of Mechanical Engineering, University of Tulsa, Tulsa, OK. Member AIAA.

†Associate Professor, Department of Mechanical Engineering. Senior Member AIAA.

region.[5-10] A common procedure in these earlier predictions was to reduce or control the value of outer eddy viscosity in the crossflow-separated region to improve the agreement between predictions and data. Among these, some authors[6,7,9,10] have reported ambiguity in determining the outer length scale of the Baldwin-Lomax model[11] in the leeward crossflow-separated region. The problem is not, however, limited to the crossflow-separated region. For instance, Rakich et al.[5] found that the value of outer eddy viscosity in the Baldwin-Lomax model was "too large" even at meridian angles upstream of the initiation of crossflow separation. Moreover, even with other algebraic turbulence models such as the Cebeci-Smith[12] and Escudier[13] models that were employed by Rakich et al.[5] and Lin et al.,[8] respectively, values of outer eddy viscosity have been reported to be too large in the leeward crossflow-separated region.

In an earlier prediction by the present authors[14] of Mach 3 flow past a sphere-cone at 4 deg incidence using the Cebeci-Smith and Baldwin-Lomax turbulence models, no crossflow separation was predicted. However, when compared with measurements, the wall shear stress was underpredicted on the windward side and was overpredicted on the leeside, although the circumferential variation of surface pressure was in excellent agreement. Similar discrepancies have been reported for skin-friction predictions in other flows past axisymmetric bodies at incidence.[9,15-18] These predictions have employed both the Cebeci-Smith and Baldwin-Lomax turbulence models, including the modified Baldwin-Lomax model developed by Degani and Schiff,[6] for incompressible and supersonic flows using boundary-layer, parabolized, and full Navier-Stokes methods. Although the leeward crossflow-separated region contributes to some of the disagreement between prediction and experiment in each of these cases (except Sturek and Schiff[15] where $\alpha = 4.2$ deg), predicted circumferential distributions of pressure and shear stress angle (or surface flow direction) were generally found to be in good agreement with measured values. Other predictions of such flows using algebraic models have shown good agreement with experimental data for surface pressure and surface flow angle,[6,7,9,10] but those quantities are not good indicators of turbulence model performance,[9,14] whereas wall shear stress and heat flux most certainly are.

The grid resolution of the predictions is also an important issue. The accuracy of predicted surface pressure or shear stress angle is much less sensitive to grid refinement near the wall than is the accuracy of wall shear stress or heat flux.[14] It is now widely recognized (e.g., Refs. 9 and 14) that accurate predictions of wall shear stress or heat flux can only be achieved with normal grid spacings near the wall smaller than about one dimensionless wall unit (here N^+). Thus comparison with earlier predictions must be done carefully. Although Sturek and Schiff[15] used N^+ between 5 and 10 near the wall, the other examples of flows past axisymmetric bodies at incidence cited earlier appear to have grid resolution adequate to accurately predict wall shear stress. In summary, the results of predictions using a variety of algebraic turbulence models and solution methods indicate that the skin-friction coefficient tends to be underpredicted on the windward side of axisymmetric bodies at incidence. In the absence of crossflow separation, the skin friction tends to be overpredicted on the leeside. This strongly suggests (as also noted by Vatsa et al.[18]) that algebraic turbulence models are deficient in modeling some of the important physics of this type of flow.

In the present work, experimental distributions of eddy viscosity for bodies at incidence have been examined. This study suggested a need to modify algebraic turbulence models for bodies at incidence. Modification to the length scale of the algebraic Cebeci-Smith model are proposed and are evaluated by comparison with experimental information. These modifications were used to recompute two flows that were considered in a previous study[14] with this same PNS method.[19] Freestream conditions for these sphere-cones (cases A and B) are given in Table 1.

Turbulent Flows past Compression Corners

Turbulence models that have been used to predict supersonic and hypersonic flows past compression corners range from simple algebraic turbulence models[23] to one- and two-equation turbulence models with various modifications.[3,4,24] One conclusion that may be drawn from these predictions is that no single model has been successful in predicting most of the cases considered. Most of the aforementioned studies examined cases for which separation occurred at the corner. However, even for cases when the flow does not separate, it is not clear whether upstream history effects are significant. Horstman[3] predicted surface pressure and heat transfer rate for a 15-deg hollow-cylinder-flare and a 15-deg compression wedge, employing Cebeci-Smith, Baldwin-Lomax, and k-ϵ models. Although all models gave the same pressure results, they showed significant differences in the heat-transfer predictions. However, in predicting the same cases as Horstman, Vuong and Coakley[4] found significant differences between the algebraic models and a two-equation q-ω model even for surface pressure.

In this study, the half-equation turbulence model developed by Johnson and King[25] was employed to predict the significance of flow history effects for a cone-cylinder-flare with 15-deg flare angle[22] using a PNS method.[19] The experimental information for this case is similar to that for the hollow-cylinder-flare with 15-deg flare angle studied by Horstman[3] and Vuong and Coakley.[4] The examination of this flow was expected to overcome perceived deficiencies in an earlier study[26] of flow past blunt 10.5-deg/7-deg and 10.5-deg/14-deg biconics that showed no significant differences between equilibrium models and the nonequilibrium Johnson-King model. Freestream conditions for this case (case C) are also given in Table 1.

Turbulence Modeling

Algebraic turbulence models are attractive because of their efficiency, simplicity, and robustness. An evaluation of two popular algebraic models for supersonic and hypersonic flows was presented by Shirazi and Truman.[14] These models would not be expected to be suitable for flows with rapid changes in the flowfield. To extend algebraic models to flows with large changes in pressure and sudden changes in body shape, nonequilibrium effects such as convection and diffusion of turbulence should be considered. A number of half-equation models appear to be suitable for use with the PNS and NS codes because of their efficiency. These models are generally characterized by an ordinary differential equation (ODE) that describes the transport of a scalar turbulent quantity in the primary flow direction. A description of several half-equation turbulence models is given in Ref. 27.

Table 1 Geometry and freestream conditions of the cases considered

Case	Geometry	$\tilde{R}_n$, in.	θ_c, deg	M	α, deg	$Re_\infty/\tilde{L}$, per ft	$\tilde{T}_\infty$, °R	$\tilde{p}_\infty$, lb/in.^{2}	$\tilde{T}_w$, °R	Ref.
A	Sphere-cone	0.65	7	3	4	2.14×10^6[a]	203	0.40	adiabatic	20
B	Sphere-cone	0.5	7	8	10	3.7×10^6	98	0.083[a]	540	21
C[c]	Cone-cylinder-flare[b]			9.22	0	14.3×10^6	116	0.366[a]	531	22

[a] Calculated from other freestream conditions given in the table.
[b] Conical nose, $\theta_c = 10$ deg; flare angle, $\theta = 15$ deg.
[c] For case C, the test gas was N_2; the test gas was air for other cases.

The extension of the PNS code to turbulent flow calculations has been discussed by Shirazi and Truman[14,28]; only a brief description is given herein. The dimensionless effective viscosity and thermal conductivity used in the PNS code are defined as

$$\mu_e = \mu_t + \mu \tag{1}$$

$$K_e = \left[(\mu_t Pr)/Pr_t\right] + K \tag{2}$$

where μ_t is the dimensionless turbulent viscosity. The turbulent Prandtl number was assumed to be $Pr_t = 0.9$. The turbulent viscosity coefficient μ_t was obtained from the Cebeci-Smith, modified Cebeci-Smith, and Johnson-King models, each of which is described below.

Cebeci-Smith Turbulence Model

The algebraic turbulence model developed by Cebeci and Smith[12] (CS) was used in the present study. The inner eddy viscosity in dimensionless form is

$$\mu_{ti} = Re_\infty \rho(\kappa N D)^2 \left|\frac{\partial V_T}{\partial N}\right| \tag{3}$$

where N is the local distance measured normal to the surface and $\kappa = 0.4$ is the von Kármán constant. The van Driest damping D is given, in dimensionless form, by

$$D = 1 - \exp\left[-N^+(\rho/\rho_w)^{1/2}(\mu_w/\mu)/A^+\right] \tag{4}$$

where N^+, the dimensionless wall coordinate, is

$$N^+ = Re_\infty^{1/2}(\tau_w/\rho_w)^{1/2}N/\nu_w \tag{5}$$

and $A^+ = 26$ is an empirical constant.

The outer-layer eddy viscosity in the CS model is described by the Clauser-Klebanoff formulation, which in dimensionless form is

$$\mu_{to} = Re_\infty(0.0168)\rho(V_T)_e\delta^*\gamma \tag{6}$$

where $(V_T)_e$ is the tangential velocity component (including crossflow) evaluated at the edge of the boundary layer δ. Definition of the boundary-layer edge for isothermal-wall and adiabatic-wall cases is given in Ref. 14.

The kinematic displacement thickness δ^* was obtained from the expression[12] for flow past an axisymmetric body of radius r_b

$$\delta^* = -r_b + \left[(\delta + r_b)^2 - 2\int_{r_b}^{\delta + r_b}(u/u_e)r\,dr\right]^{1/2} \tag{7}$$

where

$$r = (y^2 + z^2)^{1/2} \tag{8}$$

is the local radius and u_e is the velocity in the x direction evaluated at δ. The Klebanoff intermittency factor in Eq. (6) is given by

$$\gamma = 1/\left[1 + 5.5(N/\delta)^6\right] \tag{9}$$

This intermittency factor models the decrease in eddy viscosity at the edge of the boundary layer for subsonic flows. The Klebanoff intermittency factor for some of the cases considered herein was replaced by $\gamma \equiv 1$ as a first-order approximation to the intermittency distribution for hypersonic flows. Further details of this approximation are given in Refs. 14 and 29. The turbulent viscosity coefficient in Eqs. (1) and (2) was obtained from

$$\mu_t = \begin{cases} \mu_{ti} & N \le N_c \\ \mu_{to} & N > N_c \end{cases} \tag{10}$$

where N_c is the smallest value of N where $\mu_{ti} = \mu_{to}$.

Modification of Algebraic Turbulence Model for Bodies at Incidence

As discussed in the Introduction, predictions of three-dimensional turbulent flows on bodies at incidence have shown the performance of algebraic turbulence models to be deficient. Predictions reported in the literature, including some made with the present PNS code and algebraic turbulence models,[14] indicate that the eddy viscosity may be underpredicted on the windward side and overpredicted on the leeward side. The laser-Doppler velocimeter (LDV) measurements of Yanta and Ausherman[30] and hot-wire measurements of Patel and Baek[31] for bodies at incidence were considered in the present work to modify the CS turbulence model for three-dimensional effects.

Ausherman and Yanta[32] and Yanta and Ausherman[30] measured supersonic ($M = 3$) turbulent flows past spherically blunted and sharp cones with 7-deg half-angles with a two-component LDV. The eddy viscosity was calculated from measurements of Reynolds shear stress and from velocity gradients that were obtained by curve fits to the measured time-mean velocity profiles.[30] These "measured" values of eddy viscosity were normalized by "measured" displacement thickness and measured edge velocity to obtain $\tilde{\nu}_t/\tilde{\delta}^*\tilde{u}_e$. The "measured" displacement thickness was obtained from a power-law representation of the measured velocity profile with the boundary-layer edge determined from turbulent-intensity profiles.[30] This normalized eddy viscosity, when compared with the outer formulation of the Cebeci-Smith model [see Eq.(6)], should be approximately equal to the Clauser constant 0.0168 near the wall and should decrease according to the Klebanoff intermittency across the boundary layer. For cones at zero incidence, the "measured" values of eddy viscosity did show this behavior.[30,32] "Measured" distributions of eddy viscosity in flows at incidence, however, showed significant variation with meridian angle and angle of attack. The normalized eddy viscosity ($\tilde{\nu}_t/\tilde{\delta}^*\tilde{u}_e$) was significantly less than the Clauser constant on the leeward side and was much larger than the Clauser constant on the windward side; this discrepancy increased with angle of attack.

To illustrate this phenomenon, these data are presented herein in a slightly different form than that originally presented by Yanta and Ausherman.[30] The "measured" eddy-viscosity distributions are shown in Fig. 1 along with a "predicted" eddy-viscosity distribution that results from the Clauser-Klebanoff formulation in the CS model (i.e., $\tilde{\nu}_t = 0.0168\,\tilde{\delta}^*\tilde{u}_e\gamma$). The experimental values of displacement thickness $\tilde{\delta}^*$ and edge velocity $\tilde{u}_e$ were used to compute the latter. Recognizing that these values have a large uncertainty, Fig. 1 shows that the variation of "measured" eddy viscosity with respect to meridian angle is relatively small while the values "predicted" using the "measured" $\tilde{\delta}^*$ and $\tilde{u}_e$ show a large variation from the windward ($\phi = 0$ deg) to leeward ($\phi = 180$ deg) meridians. The "predicted" eddy viscosity increases from the windward to leeward sides because the displacement thickness increases from the thin boundary layer on the windward side to the thick boundary layer on the leeside; the variation in edge velocity is small. Similar behavior was observed in experimental data for the sharp cone at 2-deg incidence and for the blunt-nosed cone at 2- and 4-deg angles of attack.[32] The latter is case A considered herein.

Several conclusions might be drawn from Fig. 1. One is that the Clauser constant 0.0168 does not hold for three-dimensional flow upon bodies at angle of attack. Proper modeling of the eddy viscosity may require that it be replaced by a function of meridian angle and angle of attack. Such modification,

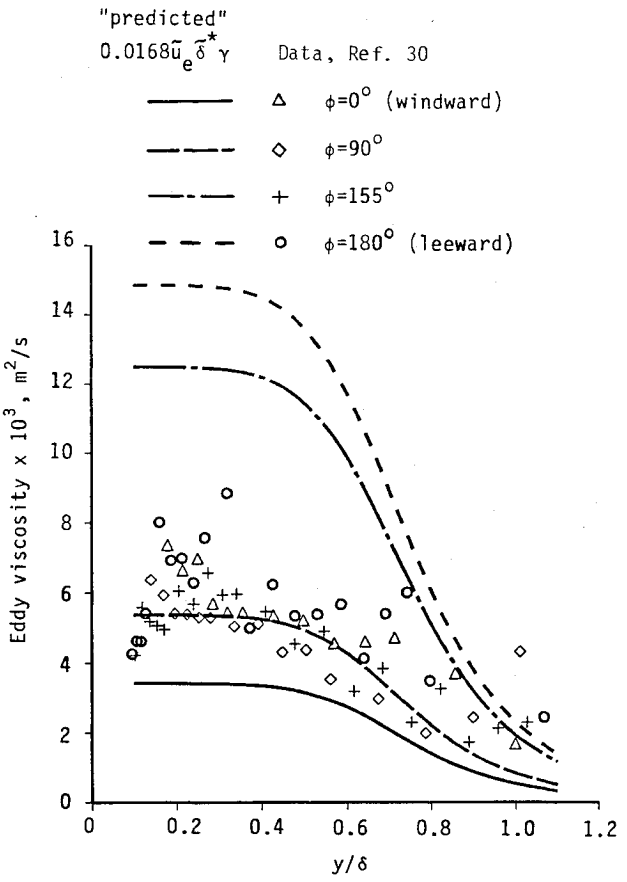

Fig. 1 "Measured" and "predicted" eddy viscosity vs distance from wall (sharp-cone: $\theta_c = 7$ deg, $M = 3$, $\alpha = 4$ deg).

however, requires substantial empirical information that is not available. Another possibility may be that using the displacement thickness as the length scale in this algebraic model is not appropriate. No other choice for the length scale is obvious. The length scale based on vorticity distribution used in the Baldwin-Lomax model[11] follows the same trend.[14] It might also be concluded that three-dimensional and possibly anisotropic effects are not properly modeled by the algebraic model. The latter was studied further by examining an entirely different set of data.

A set of turbulent flow measurements on windward and leeward planes of symmetry was recently reported by Patel and Baek.[31] The authors made subsonic turbulent flow measurements for an axisymmetric body at 15-deg incidence. Their "measured" normalized eddy viscosity on the leeside plane of symmetry was markedly smaller than the Clauser constant 0.0168. Although the measurements were inadequately resolved on the windward side, the authors indicated there was some evidence that the maximum normalized eddy viscosity may be larger than 0.0168. Patel and Baek concluded that there was a significant influence upon turbulent flow properties by extra strain rates in the mean-flow divergence (on the windward side) and convergence (on the leeside). The extra strain rates are those strain rates that are not included in the Boussinesq eddy-viscosity form because they are small relative to the main rate of strain. The effect of these extra strain rates on the Reynolds shear stress is, however, about one order of magnitude larger than their size relative to the main rate of strain.[33] A modification to account for extra-strain-rate effects is discussed below.

Modification To Account for Length Scale

To verify the observations made for the eddy-viscosity distributions discussed earlier, a simple ad hoc modification to the length scale was made to examine its influence on the mean-flow velocity and wall shear stress predictions. This simple modification to the Cebeci-Smith model, denoted by SMCS, was to use the value of displacement thickness at yaw ($\phi = 90$ deg) as the length scale at all meridian angles in the CS outer eddy viscosity, Eq. (6). This length scale was chosen since Fig. 1 indicates that the predicted eddy-viscosity profile at the yaw plane ($\phi = 90$ deg) was in good qualitative agreement with measured eddy-viscosity profiles for all meridian angles ϕ. This modification is not expected to be generally applicable; it was used herein simply to examine the effect upon the predicted velocity profiles and shear stress.

Modification for Extra Strain Rate

An alternate modification to the Cebeci-Smith model to account for extra strain rates caused by crossflow divergence and convergence was adapted from the Bradshaw extra-strain-rate model. Bradshaw[33] proposed an empirical modification to obtain an apparent mixing length that accounts for strain rates other than the main rate of strain. The usual definition of eddy viscosity includes only the gradient of streamwise velocity with respect to the normal direction, or $\partial u/\partial y$ in the classical boundary-layer notation. The modification extends the Boussinesq eddy-viscosity concept to complex turbulent flows. For the mixing length ℓ the Bradshaw formula is

$$\frac{\ell}{\ell_0} = 1 + \bar{\alpha}\frac{\text{extra strain rate}}{\text{main rate of strain (e.g., } \partial u/\partial y)} \tag{11}$$

where ℓ_0 is the mixing length without extra-strain effects, and $\bar{\alpha}$ is an empirical "constant" of order 10. Patel and Baek[17] suggested that the circumferential gradient of crossflow velocity, which is related to the rate of convergence and divergence of flow on the leeward and windward sides, respectively, is the extra rate of strain. Thus the extra rate of strain in Eq. (11) was assumed to be

$$\text{extra strain rate} = \frac{1}{r}\frac{\partial W}{\partial \phi} \tag{12}$$

where ϕ is the meridian angle, W is the crossflow velocity, and r is the local radius given by Eq. (8). For flows with no crossflow separation, the crossflow velocity increases from the windward plane toward the yaw plane and then decreases toward the leeward plane. Thus in this formulation, the mixing length and eddy viscosity are decreased on the leeside (where the extra strain rate is negative due to flow convergence) and are increased over usual values on the windward side (where the extra strain rate is positive due to flow divergence).

Since the ratio of eddy viscosities is proportional to the square of the ratio of the mixing lengths, the modified eddy viscosity μ_t^* was written as

$$\frac{\mu_t^*}{\mu_t} = \left[1 + \bar{\alpha}\frac{(1/r)(\partial W/\partial\phi)}{(\partial V/\partial N)}\right]^2 \tag{13}$$

The value of the empirical constant $\bar{\alpha}$ was taken as 10 to study the effect of this modification; this value is not expected to be a universal constant. As suggested by Bradshaw, upper and lower bounds of 1.5 and 0.5 were assumed for the term inside the bracket in Eq. (13). Outside the boundary layer where $(\partial V/\partial N)$ becomes very small, the term inside the bracket was assumed to be unity. The previous form was used to modify the CS model eddy viscosity; this model will be referred to as the modified Cebeci-Smith model with extra-strain-rate effect (MCSES). The extra-strain term given by Eq. (12) was expressed[29] in terms of the nonorthogonal coordinates used in the PNS algorithm.

Extended Form of the Johnson-King Model

In previous work,[26] the Johnson-King (JK) model[25] was extended to a three-dimensional solution procedure with a general nonorthogonal coordinate system; only a brief description

is given herein. The JK model assumes the turbulent eddy viscosity to have the functional form

$$\mu_t = \mu_{to}\left[1 - \exp(-\mu_{ti}/\mu_{to})\right] \tag{14}$$

The JK inner formulation has the dimensionless form

$$\mu_{ti} = Re_\infty^{1/2}\rho\kappa N D^2 \tau_m^{1/2} \tag{15}$$

where τ_m is the maximum total Reynolds shear stress across the boundary layer divided by density. The total Reynolds shear stress is assumed to have the dimensionless form

$$\tau = \frac{\mu_t}{\rho}\left[\left(\frac{\partial U}{\partial N}\right)^2 + \left(\frac{\partial W}{\partial N}\right)^2\right]^{1/2} \tag{16}$$

where U, the velocity tangent to the surface (excluding crossflow), was computed by removing from the total velocity the component normal to the body surface and the crossflow component W. The van Driest damping has the same form as in the CS model

$$D = 1 - \exp\left[-N^+(\rho/\rho_W)^{1/2}(\mu_W/\mu)/\mathbf{A}^+\right] \tag{17}$$

with $\mathbf{A}^+ = 15$ to account for the different velocity scale in Eq. (15).[25]

The outer-layer formulation in the JK model is

$$\mu_{to} = \sigma\left[Re_\infty(0.0168)\rho(V_T)_e\delta^*\gamma\right] \tag{18}$$

which is similar to that in the CS formulation given by Eq. (6) with the additional factor σ to account for nonequilibrium effects. The expressions for the kinematic displacement thickness and the Klebanoff intermittency factor are the same as in the CS model. The modeling parameter σ in Eq. (18) is computed for each radial ray around the circumference of the body; its variation in the streamwise direction is computed with an ordinary differential equation (ODE), or half-equation, proposed by Johnson and King[25] to describe the streamwise development of the maximum total Reynolds shear stress τ_m.

The extension[26] of this ODE to three-dimensional flow used assumptions similar to those made by Johnson and King. The ODE in dimensionless form is then

$$\underset{\text{dissipation}}{\tau_m^{1/2}} = \underset{\text{production}}{(\tau_{eq})_m^{1/2}} - \underset{\text{convection}}{Re_\infty^{1/2}\frac{L_m V_m}{a_1\tau_m}\frac{d\tau_m}{ds}} - \underset{\text{diffusion}}{\frac{L_m C_{diff}\tau_m^{1/2}\left|1-\sigma^{1/2}\right|}{a_1\delta[0.7 - N_m/\delta]}} \tag{19}$$

The subscript m in Eq. (19) denotes a quantity evaluated at the location of the maximum total Reynolds shear stress within the boundary layer. The maximum Reynolds shear stress τ_m and its location N_m were determined by interpolation within the discrete τ and N distributions along each ray ($\phi = \text{const}$). The dissipation length scale L_m was given by

$$L_m = \begin{cases} 0.4N_m, & N_m \le 0.225\delta \\ 0.09\delta, & N_m > 0.225\delta \end{cases} \tag{20}$$

In Eq. (19) the empirical constants $a_1 = 0.25$ and $C_{diff} = 0.5$ were used.

The term $d\tau_m/ds$ in Eq. (19) is the streamwise variation of the maximum total Reynolds shear stress. This term, which can be written as

$$\frac{d\tau_m}{ds} = \nabla\tau_m \cdot \boldsymbol{e}_s = \left[\frac{u}{V}\frac{\partial\tau}{\partial x} + \frac{v}{V}\frac{\partial\tau}{\partial y} + \frac{w}{V}\frac{\partial\tau}{\partial z}\right]_m \tag{21}$$

includes the crossflow variation of the maximum total Reynolds stress. Thus Eq. (19), in a general coordinate system, is a partial differential equation. References 26, 29, and 34 include detailed discussions of the implementation of the Johnson-King (JK) model and its extension to three-dimensional flows.

The nonequilibrium Johnson-King model[25] is based on differences from a corresponding equilibrium model that are caused by convection and diffusion of turbulent Reynolds stress. Thus the quantity $(\tau_{eq})_m$ in Eq. (19) was determined from the equilibrium eddy-viscosity distribution described by

$$\mu_{t,eq} = \mu_{to,eq}\left[1 - \exp(-\mu_{ti,eq}/\mu_{to,eq})\right] \tag{22}$$

$$\mu_{ti,eq} = Re_\infty^{1/2}\rho\kappa N D^2 (\tau_{eq})_m^{1/2} \tag{23}$$

$$\mu_{to,eq} = Re_\infty(0.0168)\rho(V_T)_e\delta^*\gamma \tag{24}$$

where $(\tau_{eq})_m$ is the maximum value within the τ_{eq} distribution. The values of τ_{eq} are obtained from Eq. (16) with μ_t replaced by $\mu_{t,eq}$. The eddy-viscosity distribution described by Eqs. (22–24) will be referred to as the equilibrium Johnson and King (EQJK) model.

The JK model described above accounts for nonequilibrium effects through the ODE for maximum Reynolds stress. This influence is introduced to the eddy-viscosity distribution through the parameter σ in the outer eddy-viscosity formulation. In each marching step a value of σ must be obtained for each radial ray such that the value of τ_m obtained from the eddy-viscosity distribution given by Eqs. (14–18) agrees with the value obtained from the ODE. Thus nonequilibrium effects are taken into account since the ODE accounts for convection and diffusion of the maximum Reynolds shear stress. Since the equations that describe the JK model are nonlinear in σ, τ_m, and N_m, an iterative procedure is required. An explicit procedure was used to integrate the ODE through each marching step to obtain the value of τ_m. An iterative procedure was then used to obtain values of σ and N_m at each marching step. Newton's method was used to determine σ from the nonlinear equations given by Eqs. (14–18) evaluated at N_m. The details of the solution method are described in Refs. 29 and 34.

Comparison of the nonequilibrium Johnson-King (JK) eddy-viscosity distribution with that of the CS model revealed two important differences in addition to the nonequilibrium parameter σ as discussed in Refs. 26 and 29. An increase in the outer eddy viscosity by a factor of 1.25 was made to account for the reduced eddy viscosity caused by the exponential form Eq. (14). The inner-layer damping term also used $\mathbf{A}^+ = 14$, which was found to give good agreement between the CS and EQJK models for hypersonic equilibrium (zero pressure gradient) predictions of wall shear stress and heat transfer. Similar adjustments have been used by Johnson and King.[25] The EQJK and JK models with these two modifications are hereafter denoted by MEQJK and MJK.

Numerical Solution and Grid Spacing

The generalized-coordinate PNS code used in this study was developed by Tannehill et al.[19] The extension of this code to turbulent flow calculation was discussed by Shirazi and Truman.[14,28] The Tannehill PNS code uses the Vigneron subsonic sublayer approximation[35] to the streamwise pressure gradient for stable marching. This PNS code is first-order accurate in the marching direction ξ and second-order accurate in the η (radial or normal) and ζ (circumferential) directions. Explicit fourth-order smoothing and implicit second-order smoothing terms may be used in the Tannehill PNS code to damp oscillations associated with the numerical solution algorithm. Such smoothing terms can, however, result in large errors in the prediction of heat transfer.[14,36] Shirazi and Truman[14] have demonstrated that the effect of explicit smoothing upon heat-transfer predictions will be negligible with sufficiently small values of the explicit smoothing parameters and a large number of grid points in the radial (or normal, η) and circumferential directions; no implicit smoothing was necessary.

For the present numerical results, the computational planes were chosen normal to the body axis x or ξ. The η (radial) lines were generated using straight-line rays emanating from the body that were uniformly distributed in the ζ (circumferential) direction. Radial grid points were clustered near the wall according to a stretching parameter β.[19] The step size in the marching direction grew geometrically as $\Delta\xi_{i+1} = \Gamma\Delta\xi_i$, where Γ is the step-size multiplier. This nonuniform axial grid spacing was used near the start of the calculation. For the case of the cone cylinder flare, nonuniform axial grid spacings were reclustered at the cone-cylinder and cylinder-flare junctures to adequately resolve the large gradients in the flowfield downstream of the junctures.

The accuracy of the numerical solution was carefully demonstrated by independently refining the grid in the marching, radial, and circumferential directions. The procedure, which is described by Blottner,[37] used successive grid refinement coupled with Richardson extrapolation to show the first-order accuracy in the marching direction and second-order accuracy in the radial and circumferential directions. The truncation error with respect to each direction was estimated to be about 1% or less. Further details of this procedure and the numerical solution are given in Shirazi and Truman[14] and Shirazi.[29] For cases A and B, values of N^+ nearest the wall were about one or less at the end of the marching steps. For case C, the value of N^+ nearest the wall was about 0.7 at the cylinder-flare juncture and increased to about 4 on the flare at the end of the body.

Values of all parameters that describe the grid spacing and the explicit smoothing parameter in each case are given in Tables 2 and 3. For case C, the value of the smoothing parameter at each marching step was reduced gradually to nearly zero at the end of the marching steps. This was achieved by taking the explicit smoothing parameter to be a fraction of the value at the previous marching step. The value of the explicit smoothing parameter at the start of marching solution was 0.1 and the multiplier 0.99 was used in each marching step. Thus the value of the smoothing parameter at the cylinder-flare juncture (after 1500 steps) was reduced to about 10^{-8}, and at the end of the body (after another 1000 steps) was about 10^{-12}. The last column in Table 3 is a factor of safety for the coefficient of the pressure gradient in the Vigneron approximation (see Tannehill et al.[19]).

Table 2 Input parameters for PNS predictions

Case	Initial ξ, in.[a]	Final ξ, in.[a]	ξ steps[a]	$\Delta\xi_1$, in.	Γ[b]
Sphere-cones					
A	0.573	15.555	2000	2.07×10^{-3}	1.0011
B	0.439	35.0	2000	1.29×10^{-3}	1.002
Cone-cylinder-flare					
C					
cone	2.307	6.979	500	4.82×10^{-4}	1.009
cylinder	6.979	24.971	1000	6.18×10^{-4}	1.005
flare	24.971	28.121	1000	4.78×10^{-5}	1.006

[a] ξ = streamwise, along body axis.
[b] $\Delta\xi_{i+1} = \Gamma\Delta\xi_i$.

Table 3 Input parameters for PNS predictions

Case	NK, η pts.[a]	NJ, ζ pts.[a]	β	$\epsilon_{E\eta}$[b]	Ω[c]
A	89	45	1.001	0.0045	0.9
B	89	45	1.002	0.0035	0.9
C	89	5	1.001	[d]	0.8

[a] η = normal to the body axis, ζ = circumferential.
[b] $\epsilon_{E\eta}$ = coefficient of the fourth-order explicit smoothing.
[c] Safety factor on the Vigneron coefficient of the pressure gradient near the wall.
[d] Smoothing decreased from an initial value of 0.1 to about 10^{-12} at the end of marching steps (smoothing multiplier = 0.99; total number of ξ steps = 2500).

Results

Improved predictions with algebraic turbulence models for flows over bodies at incidence will be discussed first. Then predictions of the nonequilibrium Johnson-King model will be compared with those from the algebraic Cebeci-Smith model for hypersonic flow with significant streamwise pressure gradient. Computation time for a typical turbulent flow prediction with an algebraic turbulence model was approximately 4×10^{-3} CPU seconds per grid point on a CDC Cyber 855 with NOSVE operating system. Computational time for the nonequilibrium JK model was about 10% greater. A perfect-gas model has been used to represent the properties of air and N_2. A ratio of specific heats of 1.4 and $Pr = 0.72$ were assumed in all cases.

Flows past Bodies at Incidence

The Cebeci-Smith (CS) and Baldwin-Lomax turbulence models were previously[14] found to be deficient in predicting supersonic flows at angle of attack. This was quite pronounced in the prediction of wall shear stress in the $M = 3$, $\alpha = 4$ deg case (case A). The above modifications to the algebraic CS model for bodies at incidence were used for cases A and B.

Simple Modification to the Length Scale

The simple modification to the Cebeci-Smith model (SMCS) discussed earlier was used to show the effect of the modified length scale on the predictions for cases A and B. Measured and predicted circumferential distributions of wall shear stress for flow past a spherically blunted cone at $M = 3$ and 4-deg incidence (case A) are shown in Fig. 2. Although no uncertainties were reported, the uncertainty in these wall shear stress measurements is believed[14] to be at least 10%. The wall shear stress predicted by the SMCS model shows better agreement with experimental data than that obtained using the CS model. This modification increased the outer eddy viscosity on the windward side by about 30% and decreased the outer eddy viscosity on the leeward plane by about 50%. The tangential velocity predicted by the SMCS model (not shown) indicated somewhat better agreement with experimental data at $\phi = 0$ and 135 deg than did the CS model. The SMCS model used herein can be considered a first-order correction to the length scale in the eddy-viscosity distribution in this three-dimensional flow. Although not shown here, SMCS model predictions for case B were similar to those for case A; predicted heat transfer increased on the windward side and was also somewhat improved on the leeside. Further details of this solution are given in Ref. 29.

Modification Based on Bradshaw's Model

The modified Cebeci-Smith model that accounts for extra-strain-rate effects (MCSES) was used herein to show the effect

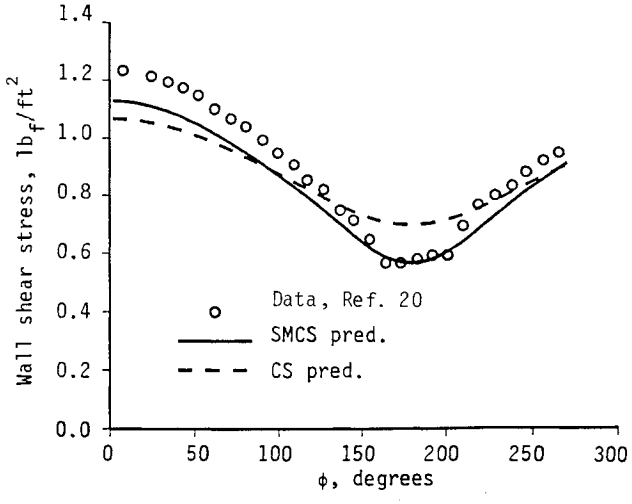

Fig. 2 Wall shear stress vs meridian angle; $M = 3$, $\alpha = 4$ deg, $\bar{x} = 15.6$ in. (case A).

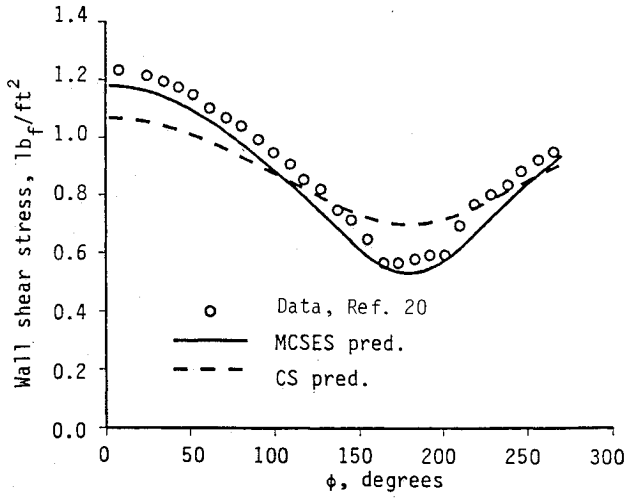

Fig. 3 Wall shear stress vs meridian angle; $M=3$, $\alpha=4$ deg, $\tilde{x}=15.6$ in. (case A).

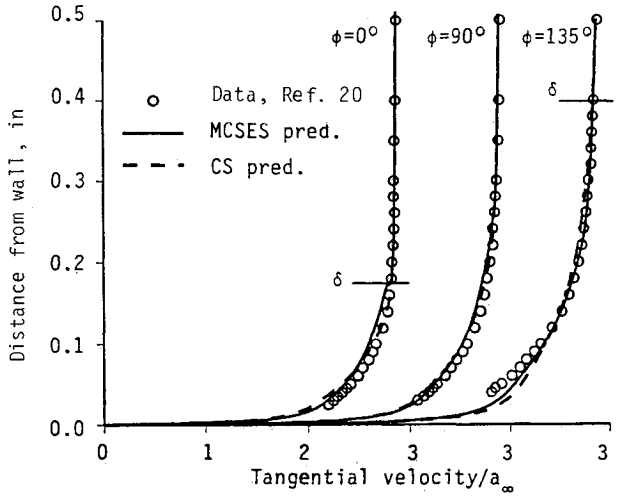

Fig. 4 Tangential velocity vs distance from wall; $M=3$, $\alpha=4$ deg, $\tilde{x}=15.6$ in. (case A).

of the extra strain rate due to crossflow divergence (on the windward side) and convergence (on the leeward side). Predicted and measured circumferential distributions of wall shear stress for case A are shown in Fig. 3. The prediction of wall shear stress using the MCSES model was in substantially better agreement with the data than was the CS model prediction. The modification had little effect on the inner part of the eddy-viscosity distribution. In the outer part, however, the MCSES model showed that the extra-strain-rate term $[(1/r)(\partial W/\partial\phi)]$ was positive on the windward side, which increased the outer eddy viscosity as compared to the CS model. On the leeward side, the extra-strain-rate term was negative and thus decreased the outer eddy viscosity of the MCSES model relative to the CS model.

The measured and predicted profiles of tangential velocity U for case A are shown in Fig. 4. Near the wall, the tangential velocity predicted with the MCSES model showed somewhat better agreement with the data than did the CS model predictions. However, the effect of these small changes in velocity profiles upon the predicted wall shear stress with the MCSES model is dramatic.

Figure 5 shows the circumferential variation of the Stanton number for case B using the CS and MCSES models (both with $\gamma\equiv 1$). The Stanton number was defined as[21]

$$St_\infty = \frac{\text{heat-transfer rate at the wall}}{\tilde{\rho}_\infty \tilde{V}_\infty\left[\tilde{h}(\tilde{T}_o)-\tilde{h}(\tilde{T}_W)\right]} \qquad (25)$$

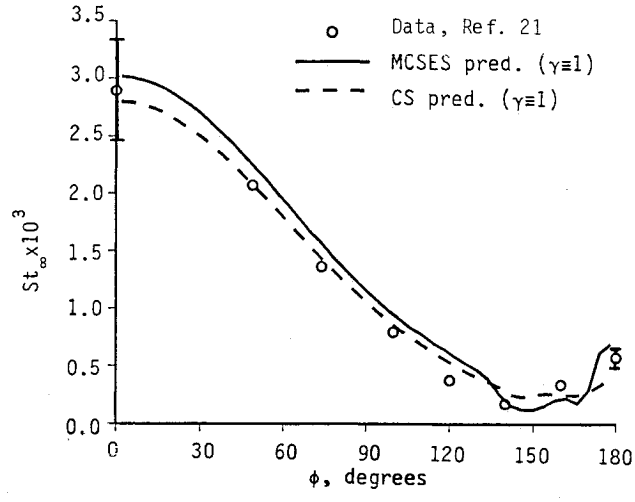

Fig. 5 Stanton number vs meridian angle; $M=8$, $\alpha=10$ deg, $\tilde{x}=28.5$ in. (case B).

where the enthalpies $\tilde{h}(\tilde{T}_W)$ and $\tilde{h}(\tilde{T}_o)$ are air-table values at the wall and freestream stagnation temperatures, respectively. On the windward side, the MCSES prediction was not substantially different than the CS prediction since the extra-strain-rate effects were small. On the leeside, however, the crossflow vortex structure caused some unusual behavior in the eddy viscosity. In the crossflow-separated region, the behavior of the crossflow velocity was quite complex. For instance, the crossflow velocity within a crossflow vortex was diverging from the leeward plane near the wall and was converging toward the leeward plane away from the surface. Then along a radial ray, the extra-strain-rate term in Eq. (13) changed sign across the crossflow vortex. This change in sign caused an abrupt change in the eddy viscosity computed from Eq. (13). This behavior of the extra-strain-rate term on the leeside is probably not physical, indicating that the relatively simple form of the Bradshaw[33] extra-strain-rate modification used herein may not be adequate in a crossflow-separated region. The simultaneous divergence near the wall and convergence in the outer portion of the leeside boundary layer of a body at incidence was noted by Patel and Baek.[17,31] It should not be surprising that the simple modification used in the MCSES model fails to accurately reproduce such a complex flow.

Analogous to previous work[5-7,9,10] in this area, eddy-viscosity distributions could be frozen at their values just upstream of the crossflow separation to avoid the above problems. Such an ad hoc modification was not considered in this study because of the limited experimental data in the crossflow-separated region. Furthermore, the results for case B obtained using the CS model without modification for extra strain rate were satisfactory. It should be noted, however, that the extra-strain-rate modification significantly improved the prediction of wall shear stress as compared to the CS model in the $M=3$, $\alpha=4$ deg case (case A) where no crossflow separation was predicted.

Performance of the Johnson-King Model

During the course of the present study, it was suspected that nonequilibrium effects may be important in the three-dimensional flows on bodies at incidence. Lin et al.,[8] for instance, argued that eddies that originated near the windward plane carried some of the character of the boundary layer on the windward side to the leeward side. To examine such an effect, a prediction using the nonequilibrium MJK model that accounts for history effects through the maximum Reynolds shear stress was made for case A. The predicted circumferential distribution of wall shear stress using the MJK model was practically the same as that predicted with the equilibrium CS model. Although the eddy viscosity predicted by both the equilibrium CS and nonequilibrium MJK models increased from

the windward side toward the leeside, strain rates decreased from the windward to the leeward sides. The net effect was that the variation in the circumferential direction of the maximum Reynolds shear stress was less than 10% for both the MEQJK and MJK models. As a result, the circumferential component of the convection term through which history effects enter the half-equation model was negligible. Since there were no significant variations in σ in the circumferential direction and its value was near unity, the MJK model gave results that were essentially the same as the equilibrium CS model. This investigation indicated that either nonequilibrium effects are not significant in this flow or that the Johnson-King model is not a good candidate to examine nonequilibrium effects for bodies at incidence. Furthermore, this illustrates that a higher-order model may not necessarily include sufficient physics to model the phenomenon of interest.

Compression Corner Flow: Isothermal Wall, $M = 9.22$, $\alpha = 0$ (Case C)

In this section, flow history effects introduced by the rapid change in streamwise flow over an axisymmetric cylinder flare are considered. The nonequilibrium Johnson-King model was considered because algebraic models cannot account for flow history effects. The experimental data[22] suggested that the flow becomes turbulent just downstream of the cone-cylinder corner. Thus nonequilibrium effects are investigated downstream of the cylinder-flare juncture. Surface pressure for the cone-cylinder-flare geometry with a 10-deg cone half-angle and 15-deg flare is shown in Fig. 6. The agreement between surface pressure predicted with the algebraic CS model and with experimental data on the cone and flare sections is within 10%. On the cylinder, however, the prediction shows somewhat larger surface pressure than that obtained experimentally. An independent prediction[38] of the surface pressure on the cone-cylinder-section for this same case using an inviscid code that employs the steady, compressible Euler equations is also shown in Fig. 6. The agreement of the present prediction with the inviscid results downstream of the cone-cylinder juncture confirms the accuracy of the present prediction. However, just downstream of the cone-cylinder juncture, where viscous effects are significant, the present prediction with the PNS code shows the trend of experimental data more accurately than the inviscid prediction.

Predictions of the wall heat-transfer rate on the flare section using the algebraic CS model and the nonequilibrium Johnson-King (MJK) model (both with $\gamma \equiv 1$) are shown in Fig. 7. Sharp gradients were predicted in the dependent variables downstream of the cylinder-flare juncture, which indicates that a strong shock was formed as a result of the compression corner. The shock, which remained within the boundary-layer region over the entire flare section, caused a small error in determining the boundary-layer edge in the CS model. The error was caused by small oscillations in the distributions of dependent variables near the shock, which are inherent in finite-difference methods employing central differencing (see Anderson et al.[27]). These small oscillations could not be eliminated even by using large explicit smoothing parameters. As the shock moved toward the edge of the boundary layer, this caused the computed edge of the boundary layer to decrease rapidly at $\tilde{x} \simeq 66.6$ cm. This reduction in boundary-layer thickness caused the displacement thickness to decrease by about 20%, which in turn reduced the CS model outer eddy viscosity. However, a CS model prediction in which the outer eddy viscosity was increased arbitrarily by 25% showed an increase in predicted heat transfer of no more than 4% downstream of the location where the rapid decrease in the boundary-layer thickness occurred. Thus the sudden decrease of the boundary-layer thickness and the corresponding decrease in outer eddy viscosity should not have a large effect on the heat-transfer prediction.

The MJK model prediction was started on the cylinder well upstream of the flare at $\tilde{x} = 28.2$ cm. Heat transfer predicted using the MJK model showed no improvement over that predicted with the algebraic CS model. Although the agreement of the CS model predictions with experimental data is actually somewhat better than that of the MJK model, both predictions lie within the estimated uncertainty in the data. (No uncertainties for the measurements were reported.) The difference between the heat transfer predicted by the CS and MJK models

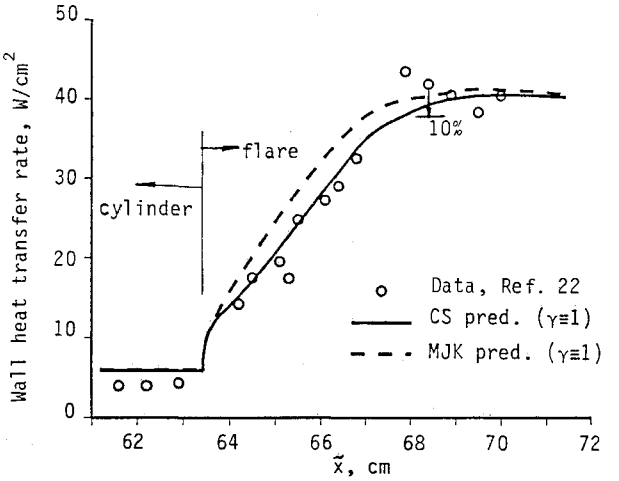

Fig. 7 Wall heat transfer rate vs body-axis distance from nose; $M = 9.22$, $\alpha = 0$ deg (case C).

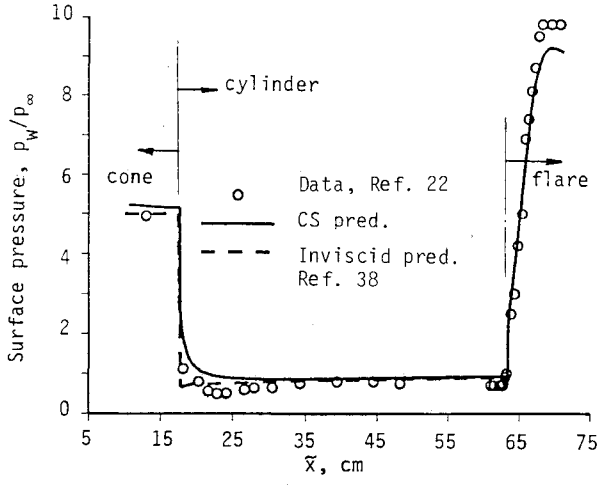

Fig. 6 Surface pressure vs body-axis distance from nose; $M = 9.22$, $\alpha = 0$ deg (case C).

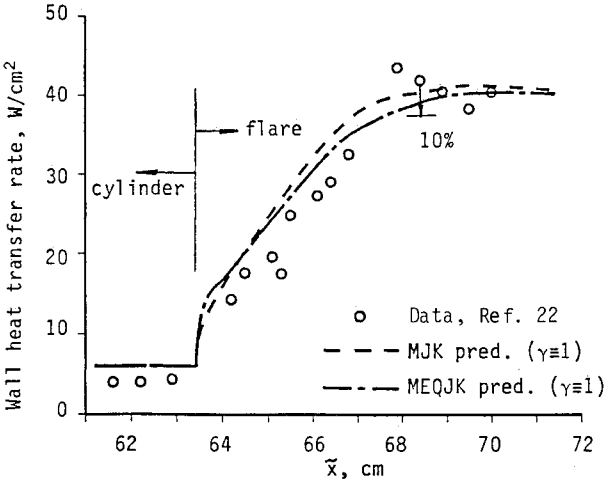

Fig. 8 Wall heat transfer rate vs body-axis distance from nose; $M = 9.22$, $\alpha = 0$ deg (case C).

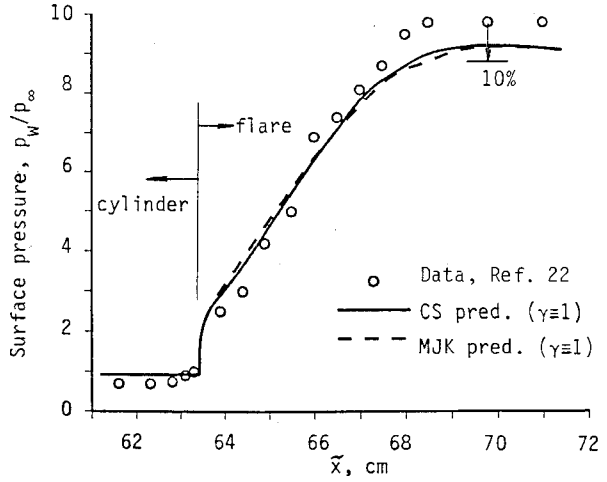

Fig. 9 Surface pressure vs body-axis distance from nose; $M = 9.22$, $\alpha = 0$ deg (case C).

just downstream of the cylinder-flare juncture was due to the parameter σ used in the outer eddy-viscosity formulation of the nonequilibrium MJK model as well as to the use of the maximum Reynolds shear stress for the velocity scale in the inner eddy-viscosity formulation of the MJK model.

To illustrate the effect of the nonequilibrium parameter σ, heat-transfer predictions using the MJK and MEQJK models are shown in Fig. 8. Downstream of the cylinder-flare juncture, the differences between the two models is attributed to the effect of σ since $\sigma \equiv 1$ in the MEQJK model. The nonequilibrium MJK model effectively prevented changes in the streamwise direction from occurring as rapidly as with the equilibrium model. However, this did not result in noticeably improved predictions. More details of the predicted parameters are given in Ref. 29; surface pressure predicted by the CS and MJK models, shown in Fig. 9, showed only small differences. The surface pressure predicted by each model agreed with experimental data to within 10% all along the flare.

Concluding Remarks

Modifications to algebraic turbulence models were proposed to improve predictions of supersonic and hypersonic flows at incidence. Both the simple length-scale modification to the CS model (SMCS) and the modification to the CS model based on the Bradshaw extra-strain-rate model (MCSES) significantly improved the prediction of wall shear stress for the $M = 3$, $\alpha = 4$ deg case (case A). In the $M = 8$, $\alpha = 10$ deg case (case B), however, it appears that these modifications are not adequate to accurately resolve the complex flow in the crossflow-separated region. Without pertinent experimental information for the eddy viscosity and Reynolds stresses in the crossflow-separated region of bodies at large incidence, little improvement in these turbulence models can be expected. The MCSES modification, which was based on experimental data with no crossflow separation, gave predictions that agreed reasonably well with measurements of wall shear stress. Further study and extensive experimental information will be required to develop a more robust turbulence model that can be applied to regions with crossflow separation.

Parabolized Navier-Stokes (PNS) predictions of turbulent flows at hypersonic speed past a cone-cylinder-flare body have been compared with measurements of heat transfer and surface pressure. These predictions were used to evaluate the nonequilibrium Johnson-King half-equation turbulence model. Predictions employing the equilibrium Cebeci-Smith and nonequilibrium Johnson-King models were both within the estimated uncertainty of the heat transfer data. The simple nonequilibrium Johnson-King model showed no significant improvement over the algebraic Cebeci-Smith model for the attached flows considered herein and in Ref. 26. That the Cebeci-Smith and Johnson-King models give similar results leads to an important conclusion from this work. Algebraic turbulence models appear to be adequate to predict supersonic and hypersonic flows as long as the flow does not experience streamwise separation.

Acknowledgments

This work was supported by the Computational Aerodynamics Division, Sandia National Laboratories, Albuquerque (SNLA), New Mexico. The encouragement of contract monitor William Oberkampf is greatly appreciated. Starting solutions were provided by Frederick Blottner, Don Larson, and Mary Walker of SNLA. Patrick Roache provided valuable advice in the preparation of the final manuscript.

References

[1]Danberg, J. E., van Gulick, P., and Kim, J., "Turbulence Modeling for Steady Three-Dimensional Supersonic Flows," U.S. Army Ballistic Research Laboratory, Aberdeen Proving Ground, MD, BRL-CR-553, June 1986.

[2]Helliwell, W. S., Alber, I. E., Dickinson, R. P., and Lubard, S. C., "Turbulent Flow Over Vehicles at Angle of Attack," *AIAA Journal,* Vol. 22, No. 3, 1984, pp. 321–322.

[3]Horstman, C. C., "Prediction of Hypersonic Shock-Wave/Turbulent-Boundary-Layer Interaction Flows," AIAA Paper 87-1367, June 1987.

[4]Vuong, S. T., and Coakley, T. J., "Modeling of Turbulence for Hypersonic Flows With and Without Separation," AIAA Paper 87-0286, Jan. 1987.

[5]Rakich, J. V., Vigneron, Y. C., and Agarwal, R., "Computation of Supersonic Viscous Flows Over Ogive-Cylinders at Angle of Attack," AIAA Paper 79-0131, Jan. 1979.

[6]Degani, D., and Schiff, L. B., "Computation of Turbulent Supersonic Flows Around Pointed Bodies Having Crossflow Separation," *Journal of Computational Physics,* Vol. 66, Sept.-Oct. 1986, pp. 173–196.

[7]Weinacht, P., Guidos, B. J., Sturek, W. B., and Hodes, B. A., "PNS Computations for Spinning Shell at Moderate Angles of Attack and for Long L/D Finned Projectiles," AIAA Paper 85-0273, Jan. 1985.

[8]Lin, T. C., Rubin, S. G., and Widhopf, G. F., "A Two-Layer Model for Coupled Three-Dimensional Viscous and Inviscid Flow Calculations," AIAA Paper 81-0118, Jan. 1981.

[9]Panaras, A. G., and Steger, J. L., "A Thin-Layer Solution of the Flow about a Prolate Spheroid," *Zeitschrift für Flugwissenschaften und Weltraumforschung,* Vol. 12, 1988, pp. 173–180.

[10]Hartwich, P.-M., and Hall, R. M., "Navier-Stokes Solutions for Vortical Flows Over a Tangent-Ogive Cylinder," *AIAA Journal,* Vol. 28, No. 7, 1990, pp. 1171–1179.

[11]Baldwin, B. S., and Lomax, H., "Thin Layer Approximation and Algebraic Model for Separated Turbulent Flows," AIAA Paper 78-0257, Jan. 1978.

[12]Cebeci, T., and Smith, A. M. O., *Analysis of Turbulent Boundary Layers,* Academic, New York, 1974, pp. 92–94, 215–217.

[13]Escudier, M. P., "The Distribution of Mixing Length in Turbulent Flows Near Walls," Mechanical Engineering Department, Imperial College of Science and Technology, Univ. of London, London, England, UK, Rept. TWF/TN/1, 1965.

[14]Shirazi, S. A., and Truman, C. R., "Evaluation of Algebraic Turbulence Models for PNS Predictions of Supersonic Flow Past a Sphere-Cone," *AIAA Journal,* Vol. 27, No. 5, 1989, pp. 560–568.

[15]Sturek, W. B., and Schiff, L. B., "Numerical Simulation of Steady Supersonic Flow over Spinning Bodies of Revolution," *AIAA Journal,* Vol. 20, No. 12, 1982, pp. 1724–1731.

[16]Cebeci, T., "Three-Dimensional Boundary Layers on Missiles," *Tactical Missile Aerodynamics,* edited by M. J. Hemsch and J. N. Nielsen, Progress in Astronautics and Aeronautics, AIAA, New York, 1986, pp. 723–777.

[17]Patel, V. C., and Baek, J. H., "Boundary Layers in Planes of Symmetry, Part II: Calculations for Laminar and Turbulent Flows," *AIAA Journal,* Vol. 25, No. 6, 1987, pp. 812–818.

[18]Vatsa, V. N., Thomas, J. L., and Wedan, B. W., "Navier-Stokes Computations of Prolate Spheroids at Angle of Attack," AIAA Paper 87-2627, Jan. 1987.

[19]Tannehill, J. C., Venkatapathy, E., and Rakich, J. V., "Numerical Solution of Supersonic Viscous Flow Over Blunt Delta Wings," *AIAA Journal,* Vol. 20, No. 2, 1982, pp. 203–210.

[20]Ausherman, D. W., Yanta, W. J., and Rutledge, W. H., "Mea-

surements of the Three-Dimensional Boundary Layers on Conical Bodies at Mach 3 and Mach 5," AIAA Paper 83-1675, Jan. 1983.

[21]Carver, D. B., "Heat Transfer, Surface Pressure and Flow Field Surveys on Conic and Biconic Models with Boundary Layer Trips at Mach 8—Phases IV and V," Calspan/Arnold Engineering Development Center Division, Arnold AFS, TN, AEDC-TSR-80-V14, March 1980.

[22]Coleman, G. T., "A Study of Hypersonic Boundary Layers Over a Family of Axisymmetric Bodies at Zero Incidence," Dept. of Aeronautics, Imperial College of Science and Technology, Univ. of London, London, England, UK, I.C. Aero Report 73-06, Sept. 1973.

[23]Ong, C., and Knight, D., "A Comparative Study of the Hybrid MacCormack and Implicit Beam-Warming Algorithms for a Two-Dimensional Supersonic Compression Corner," AIAA Paper 86-0204, Jan. 1986.

[24]Viegas, J. R., and Horstman, C. C., "Comparison of Multiequation Turbulence Models for Several Shock Separated Boundary-Layer Interaction Flows," *AIAA Journal,* Vol. 17, No. 8, 1979, pp. 811–820.

[25]Johnson, D. A., and King, L. S., "A Mathematically Simple Turbulence Model for Attached and Separated Turbulent Boundary Layers," *AIAA Journal,* Vol. 23, No. 11, 1985, pp. 1684–1692.

[26]Shirazi, S. A., and Truman, C. R., "A Study of Algebraic and Half-Equation Turbulence Models For Hypersonic PNS Predictions," AIAA Paper 88-0222, Jan. 1988.

[27]Anderson, D. A., Tannehill, J. C., and Pletcher, R. H., *Computational Fluid Mechanics and Heat Transfer,* Hemisphere, New York, 1984, pp. 468–472.

[28]Shirazi, S. A., and Truman, C. R., "Comparison of Algebraic Turbulence Models for PNS Predictions of Supersonic Flow Past a Sphere-Cone," AIAA Paper 87-0544, Jan. 1987.

[29]Shirazi, S. A., "Evaluation of Algebraic and Half-Equation Turbulence Models for Supersonic and Hypersonic Flows Using a Parabolized Navier-Stokes Method," Ph.D. Dissertation, Dept. of Mechanical Engineering, Univ. of New Mexico, Albuquerque, NM, 1989.

[30]Yanta, W. L., and Ausherman, D. W., "The Turbulent Transport Properties of a Supersonic Boundary Layer on a Sharp Cone at Angle-of-Attack," AIAA Paper 83-0456, Jan. 1983.

[31]Patel, V. C., and Baek, J. H., "Boundary Layers in Planes of Symmetry, Part I: Experiments in Turbulent Flow," *AIAA Journal,* Vol. 25, No. 4, 1987, pp. 550–558.

[32]Ausherman, D. W., and Yanta, W. J., "The Three-Dimensional Turbulence Transport Properties in the Boundary Layers of Conical Body Configurations at Mach 3," AIAA Paper 84-1528, June 1984.

[33]Bradshaw, P., "Review: Complex Turbulent Flows," *ASME Journal of Fluids Engineering,* Vol. 97, No. 2, 1975, pp. 146–154.

[34]Shirazi, S. A., and Truman, C. R., "Simple Turbulence Models for Supersonic and Hypersonic Flows: Bodies at Incidence and Compression Corners," AIAA Paper 89-0669, Jan. 1989.

[35]Vigneron, Y. C., Rakich, J. V., and Tannehill, J. C., "Calculation of Supersonic Viscous Flow over Delta Wings with Sharp Subsonic Leading Edges," AIAA Paper 78-1137, July 1978.

[36]Chaussee, D. S., "NASA Ames Research Center's Parabolized Navier-Stokes Code: A Critical Evaluation of Heat-Transfer Predictions," AIAA Paper 87-1474, June 1987.

[37]Blottner, F. G., "Investigation of Some Finite-Difference Techniques for Solving the Boundary Layer Equations," *Computer Methods in Applied Mechanics and Engineering,* Vol. 6, July 1975, pp. 1–30.

[38]Walker, M. A., personal communication, 1988.